SCIENCE CHINA
Earth Sciences

•RESEARCH PAPER•

December 2018 Vol.61 No.12: 1844–1858
https://doi.org/10.1007/s11430-018-9260-0

Numerical simulation of the influence of aerosol radiation effect on urban boundary layer

Xinran WANG[1,2], Xiaodong HE[2], Shiguang MIAO[2*] & Youjun DOU[2]

[1] *China Institute of Atomic Energy, Beijing 102413, China;*
[2] *Institute of Urban Meteorology, China Meteorological Administration, Beijing 100089, China*

Received March 29, 2018; revised May 21, 2018; accepted August 16, 2018; published online October 10, 2018

Abstract With the intensification of pollution and urbanization, the aerosol radiation effect continues to play an important role in the urban boundary layer. In this paper, a winter pollution process in Beijing has been taken as an example, and a new aerosol vertical profile in the radiative parameterization scheme within the Weather Forecast Research and Forecasting (WRF) model has been updated to study the effect of aerosols on radiation and the boundary layer. Furthermore, the interactions among aerosols, urbanization, and planetary boundary layer (PBL) meteorology were discussed through a series of numerical experiments. The results show the following: (1) The optimization improves the performance of the model in simulating the distribution features of air temperature, humidity, and wind in Beijing. (2) The aerosols reduce the surface temperature by reducing solar radiation and increasing the temperature in the upper layer by absorbing or backscattering solar radiation. The changes in the PBL temperature lead to more stable atmospheric stratification, reducing the energy transfer from the surface and the height of the boundary layer. (3) With the increase in the aerosol optical depth, the atmospheric stratification most likely becomes stable over rural areas, most likely becomes stable over suburb areas, and has great difficultly becoming stable over urban areas. Aerosol radiative forcing, underlying urban surfaces, and the interaction between them are the main factors that affect the changes in the meteorological elements in the PBL.

Keywords Aerosol, Urbanization, Boundary layer, Meteorological elements, WRF

Citation: Wang X, He X, Miao S, Dou Y. 2018. Numerical simulation of the influence of aerosol radiation effect on urban boundary layer. Science China Earth Sciences, 61: 1844–1858, https://doi.org/10.1007/s11430-018-9260-0

1. Introduction

In recent years, with the rapid development of the economy and industry, cities have faced frequent aerosol contamination accidents. Aerosols affect not only the living environment but also the characteristics of urban boundary layers through radiative forcing. Aerosol radiative forcing includes two parts: direct and indirect. Direct radiative forcing means that aerosols can cool the Earth-atmosphere system by scattering and increase the temperature by absorption (Li et al., 2017). Indirect radiative forcing means that aerosols can change the microphysical structures of clouds via the cloud condensation nuclei and thus reform the energy balance of the Earth-atmosphere system and precipitation (Ding et al., 2013; Albrecht, 1989). Studies have shown that aerosol radiative forcing not only affects the regional climate (Li et al., 1992; Li et al., 2015; Huang et al., 2006) but also significantly changes the structure of the boundary layer (Cheng et al., 2002; Pleim, 2007; Yu et al., 2002; Pandithurai et al., 2008; Wang et al., 2006) by affecting the characteristics of the planetary boundary layer (PBL) such as temperature and wind speed (Wu et al., 2014; Li et al., 2007).

Numerical simulation methods have been widely used to study aerosols. Sun et al. (2012) coupled a one-dimensional boundary layer model with a radiative transfer scheme to study the effects of aerosols on meteorological elements in

* Corresponding author (email: sgmiao@ium.cn)

the PBL. Ding et al. (2013) and Huang et al. (2016) used the WRF-Chem model (Weather Research Forecast model coupled with Chemistry) to study the effect of the interactions between aerosols and radiation on precipitation in eastern China. Wong et al. (2012) used the WRF-CMAQ model (Weather Research Forecast model coupled with Community Multiscale Air Quality) to analyze the feedback mechanism of aerosols in the atmosphere. Although a variety of models can be used to simulate aerosol distribution, the Weather Research Forecast (WRF) model, which is currently the most operational, has not been developed in this aspect and depends on only the WRF-Chem model. However, the WRF-Chem model cannot meet operation requirements because of its long operating time and complicated simulation process. Therefore, this paper plans to improve the WRF model to simulate the aerosol distribution characteristics.

With the development of society and the concentration of the population, the process of urbanization is accelerating. Studies have shown that urbanization has made important contributions to regional climate change (Liao, 2014). Wang et al. (2013) used a mesoscale model to analyze the impact of urbanization on the winter heat island of Lanzhou and found that the contribution of urbanization was approximately 44%. Wang (2017) analyzed the effect of urbanization on the precipitation in Jing-Jin-Ji and found that precipitation will increase with the expansion of cities. Liu et al. (2017) analyzed the turbulent diffusion characteristics of the urban PBL. Liao (2014) and Tao et al. (2014) found that urbanization decreased the PM_{10} concentration by 40% in July and increased the O_3 surface volume fraction in eastern China.

Beijing is a rapidly developing city with poor air quality (Che et al., 2015, 2008), and the research on the impacts of urbanization and aerosols on atmospheric stratification and meteorological elements in the PBL is lacking. Therefore, Beijing is taken as an example in this paper to optimize the radiation scheme of WRF V3.7 by introducing a new aerosol vertical profile and verifying the performance of the model. Then, the characteristics of the meteorological elements in the PBL and the effect of aerosol on the radiation and PBL are simulated using an optimized model. Furthermore, the effects of aerosols and underlying urban surfaces on atmospheric stratification were discussed through a series of numerical experiments.

2. Model and data

2.1 Case introduction

The pollution episode is from 0800 LST, December 23 to 0800 LST, December 24, 2013 (Beijing time, the same below), and there are no clouds during this period. From the analysis of the atmospheric background field, Beijing is in front of the ridge in the middle troposphere (500 hPa). Cold air is concentrated around Lake Baikal, which does not affect Beijing. At the ground surface, Beijing is influenced by a uniform pressure field. During the daytime, most areas of Beijing are influenced by northerly and north-easterly winds, and the wind speed is slow with sparse isobaric pressure lines. At night, Beijing is under the control of the east and southeast winds, and the wind speed is also slow. A pollution analysis revealed that the concentrations of $PM_{2.5}$ differ throughout the area, and these concentrations are high in the south and low in the north; the highest $PM_{2.5}$ concentration is in the southeast of Beijing (Figure 1). Figure 2 shows the daily changes in the aerosol optical depth (AOD) and meteorological elements in the PBL. In this area, the variations in the AOD are very small between 0.15 and 0.2. However, the characteristics of the daily temperature variations are obvious. The wind speed corresponds to the northeast wind during the daytime. The humidity decreases from 80% to only 25% (1600 LST) during the day and gradually increases at night. These results reflect that the pollution is localized, the wind speed is slow, and the AOD is almost consistent.

2.2 The WRF model and numerical experimental design

The WRF model is a mesoscale weather forecast model that was developed by the National Center for Atmospheric Research (NCAR), the National Center for Environmental Prediction (NCEP), and the University of Oklahoma in 1997. The horizontal resolution of the WRF model is 1–10 km and it includes a full compressible, nonhydrostatical model core. The horizontal direction adopts the Arakawa C staggered grid arrangement, and the vertical direction adopts terrain following quality coordinates. The WRF model includes one-way, two-way and moving nesting and a variety of physical schemes, focusing on solving the simulation and prediction of atmospheric conditions within a limited area within 60 hours (Tang and Jia, 2006).

The WRF model-V3.7 is used in this paper. There are four one-way nested domains (Figure 3a). The horizontal resolutions are 27, 9, 3, and 1 km. For each domain, there are 154×154, 154×154, 154×154, 184×172 horizontal grid cells and 38 layers in the vertical direction. The pressure of the highest layer is 50 hPa. The center point was selected at Tiananmen (40.24°N, 116.45°E) (Zhang et al., 2013). The initial field and boundary conditions were calculated using NCEP 1°×1° reanalysis data. The land use types in the model were updated from the USGS data of 24 land use types in the 1990s to the high-resolution Landsat-TM satellite data in 2009. The urban land use types were classified into low-density, medium-density, and high-density urban types based on the percentage of impervious areas (Zhang et al., 2013).

The main physical parameterization scheme used in this paper is shown in Table 1. To explore the radiative forcing of

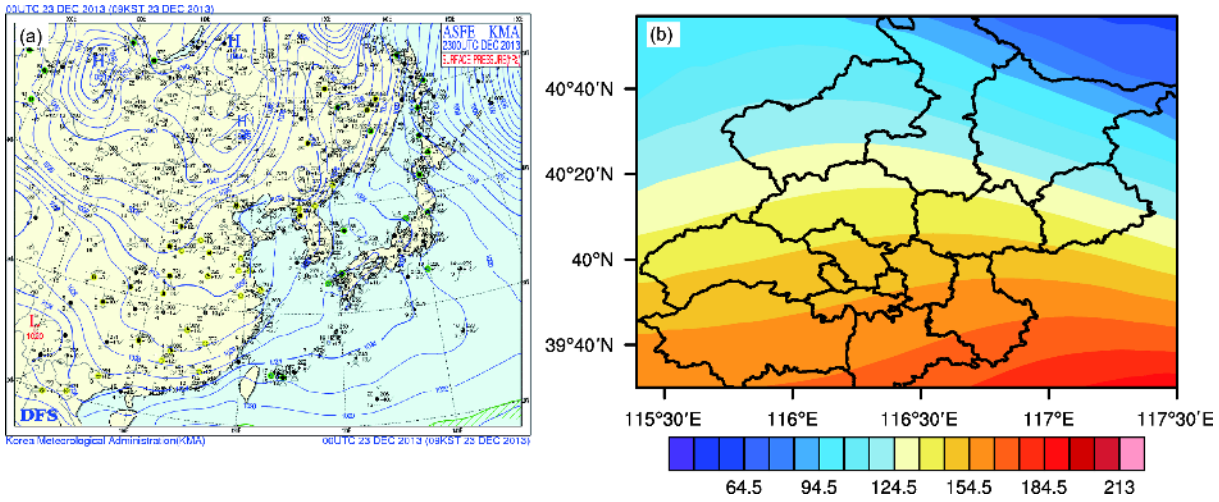

Figure 1 Weather situation and pollutant distribution in Beijing from December 23 to 24, 2013. (a) Surface weather chart at 0800 LST; (b) horizonal distribution of $PM_{2.5}$.

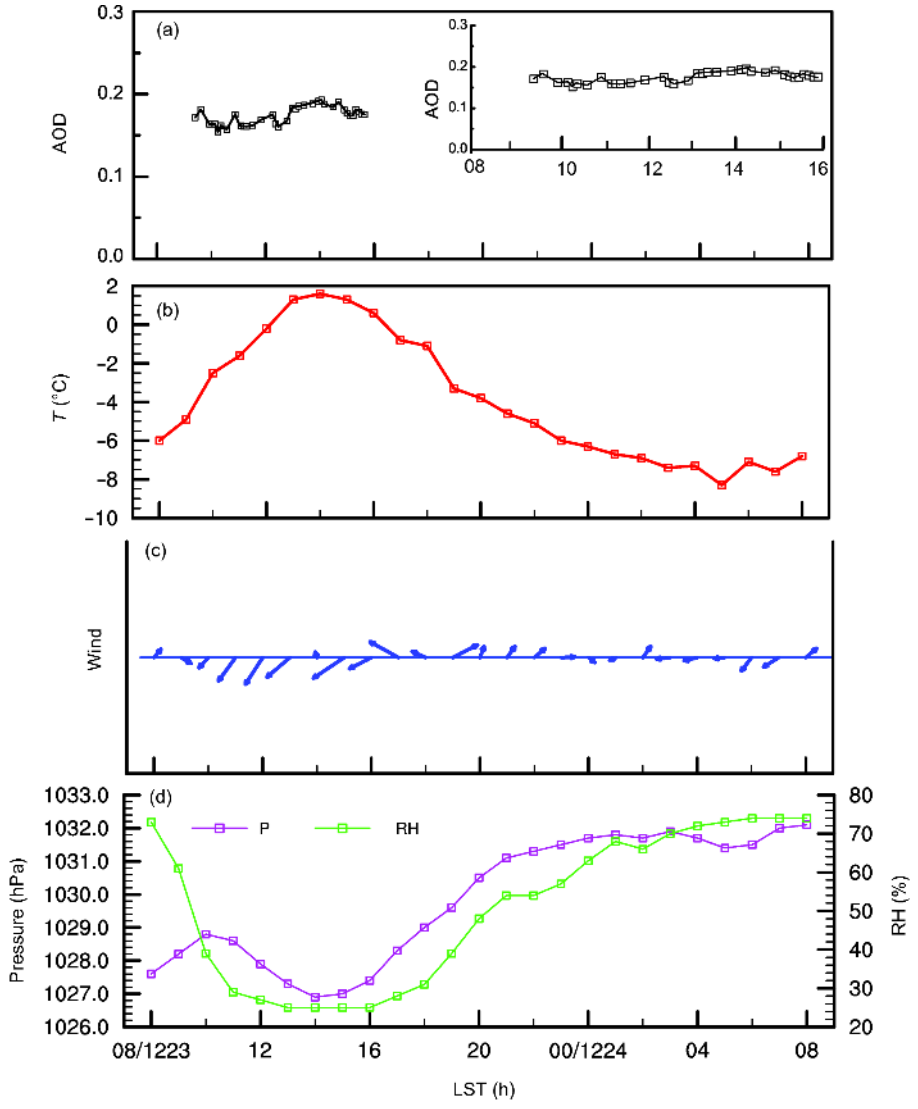

Figure 2 Daily variations in aerosols and PBL meteorology. (a) Aerosols (the small image in the top right corner is an enlarged version of AERONET-AOD); (b) temperature; (c) wind; (d) pressure and relative humidity.

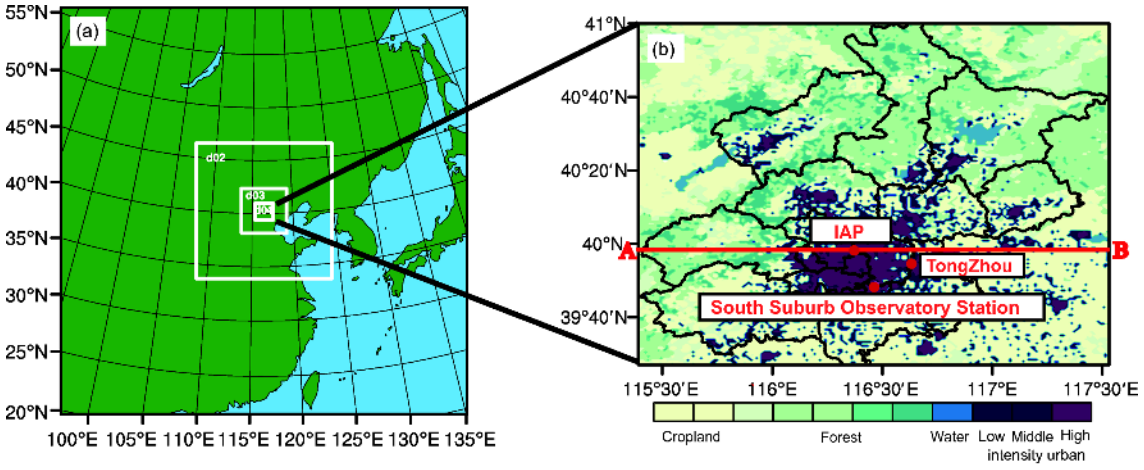

Figure 3 Study area. (a) Full area. (b) Beijing zoom-in (area of the smallest white box in (a)); with administrative boundaries (black lines), underlying surface types (shaded), the position of the latitudinal section through Institute of Atmospheric Physics (IAP) station (red line) and urban, suburban and rural sites (red dots).

aerosols, the rapid radiative transfer model for general circulation models (RRTMG) (Iacono et al., 2008) is selected by the shortwave radiation scheme. RRTMG is a new type of radiation transmission scheme developed by the American Atmospheric and Environmental Research Corporation (AER) that has high simulation accuracy and radiation efficiency. RRTMG can accurately describe the transmission process (Zhao et al., 2014; Su et al., 2016). The aerosol input is enabled in the RRTMG scheme by the option AER_OPT. This option includes no aerosol input, a climate average aerosol input, and an external aerosol 2D field input. In this study, we will first compare the effectiveness of the three opinions above and then optimize the vertical profile of the AOD of RRTMG scheme (in part 2.3). Furthermore, the effect of aerosol radiative forcing and the underlying surface on the atmospheric stratification and diffusion conditions are discussed through a series of numerical experiments. In this study, we conducted 10 numerical experiments (Table 2). The first is a control experiment (Test 1), which has no AOD input (indicated by AOD=0 in Table 2), and the next is a comparative experiment, which uses a climatological mean AOD input (expressed in terms of climatological mean in Table 2). The other experiments are designed to be sensitivity test with different values for the MODIS-AOD input (expressed by n times MODIS daily mean value in Table 2, MODIS-AOD data will be introduced in part 2.3.1).

2.3 Aerosol data

2.3.1 Daily variation data on aerosol optical depth

Aerosol Robotic Network (AERONET) Level 2.0 data are used to analyze the daily AOD variations. AERONET is an aerosol monitoring network that was established by both NASA and the National Research Center of France. The observation data have high accuracy. The AOD of each band can be obtained by inverting direct solar radiation measurements collected by sun photometers. The data are computed for three quality levels. In this paper, we selected the most reliable Level 2 data, which is quality-assured and cloud-screened, and analyze the daily variation in AOD at 675 nm at the Beijing site (the site location: 39.977°N, 116.381°E, the data from other sites are missing).

2.3.2 Data on the horizontal variation in aerosol optical depth

Daily averaged MOD08_D3 aerosol data on December 23, 2013, from the Terra satellite are used as the input data for this pollution simulation, and these data have a horizontal resolution of 1° (other high-resolution aerosol products are missing during this period). As shown in Figure 2, the daily variation in AOD is very small in Beijing. Therefore, it is reasonable to use the daily average data in this study. The horizontal distribution of MODIS-AOD is shown in Figure 4. The highest AOD is found in the southeast, while relatively low AOD values are found in the north, which is a typical characteristic of the pollutant distribution in Beijing —"Different from North to South" (Dong et al., 2013). Local pollution plays an important role in this process (seen in part 2.1). In Figure 4, M and N are two main zones located to the north and south of Beijing's Sixth Ring Road. The AOD of zone M is 0.2–0.3, and that of zone N is 0.4–0.6. Both zones can be used as contrast zones in this pollution process in Beijing.

2.3.3 Vertical variation data of aerosol optical depth

The WRF default vertical profile of the aerosol extinction coefficient is replaced by the vertically observed curve. In the default profile (Figure 5a), the aerosol extinction coef-

Table 1 Physical schemes

Physical Schemes	Scheme No.	Descriptions (References)
Microphysics	8	Thompson (Thompson et al., 2008)
Longwave radiation	4	RRTMG (Iacono et al., 2008)
Shortwave radiation	4	RRTMG (Iacono et al., 2008)
Surface layer	1	Revised MM5 Monin-Obukhov (Paulson,1970; Dyer and Hicks, 1970; Webb,1970; Beljaars,1995; Zhang and Anthes, 1982)
Land surface	2	Noah (Tewari et al., 2004)
Boundary layer	7	ACM2 (Pleim, 2007)
Urban canopy	0 (d01–d03)	No
	1 (d04)	SLUCM (Chen et al., 2011)
Cumulus clouds	0 (d03–d04)	No
	1 (d01–d02)	Kain-Fritsch (new Eta) scheme (Kain, 2004)

Table 2 Numerical experiments

Type of experiment	Test No.	Description
Control experiment	Test 1	AOD=0
Contrast experiment	Test 2	AOD=climate average AOD
Sensitivity experiments	Test 3	AOD=MODIS-AOD
	Test 4	AOD=2 times of MODIS-AOD
	Test 5	AOD=3 times of MODIS-AOD
	Test 6	AOD=3.5 times of MODIS-AOD
	Test 7	AOD=4 times of MODIS-AOD
	Test 8	AOD=4.5 times of MODIS-AOD
	Test 9	AOD=5 times of MODIS-AOD
	Test 10	AOD=5.5 times of MODIS-AOD

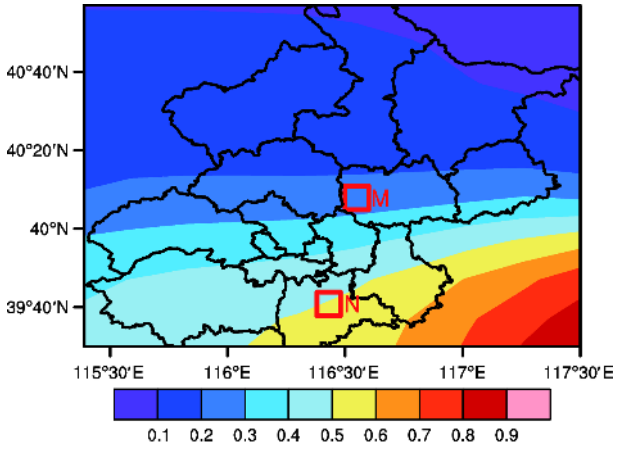

Figure 4 Daily averaged MODIS-AOD in Beijing and surrounding areas on December 23, 2013 (the two red boxes represent the two areas (M and N) with different AOD values, the same below).

ficient first increases and then gradually decreases with altitude. The highest value appears at 1–2 km. This feature is different from that observed by Liu et al. (2009) using an aircraft. Therefore, this paper imitates the vertical distribution of the aerosol concentration under heavy pollution weather observed by Zhang et al. (2009) in Beijing and replaces the vertical profile of the aerosol extinction coefficient in the model to simulate the vertical characteristics of aerosols (Figure 5b). In the new profile, the surface extinction coefficient of aerosols is the highest and the value decreases rapidly with altitude at approximately 1 km, forming a strong vertical gradient.

2.3.4 $PM_{2.5}$ data

Hourly $PM_{2.5}$ concentrations from 35 weather stations in the Beijing area from December 23 to 24, 2013, were used here to study the characteristics of this pollution process.

2.4 Meteorological observation data

The observation data used here include the temperature, pressure, humidity and wind from the observation stations of the South Suburbs, and these data are from December 23 to 24, 2013. These data are used to analyze the daily change in PBL meteorology during the pollution process. Additionally, the observation data of radiation, temperature, humidity and wind speed from the Institute of Atmospheric Physics (IAP) Station, South Suburb Observatory Station and Miyun Station are used to verify the reliability of the optimization scheme. The other meteorological data of temperature, hu-

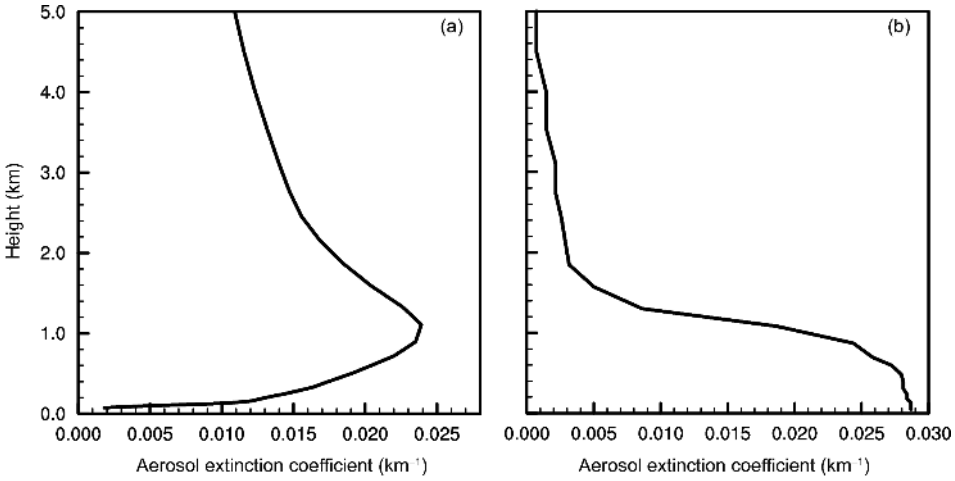

Figure 5 Vertical distributions of the aerosol extinction coefficient (km^{-1}). (a) Default vertical profile in the WRF model; (b) the new profile based on the vertical distribution of aerosol number concentration in Beijing observed under heavy pollution days.

midity and wind are selected from 295 automatic weather stations in Beijing. These data have high precision and fine timeliness, which have great significance for the study of meteorological and climatic characteristics in Beijing (Dou, 2013). More details about the site location and the radiation data are shown in Wang et al. (2016).

3. Model evaluation

To verify the reliability of the optimization scheme, three observation stations in Beijing (Wang et al., 2016) are selected here to verify the ability of the model to simulate the surface short wave flux. Figure 6 indicates that the three experiments can adequately simulate the surface short wave flux, with the maximum flux occurring at 12 noon. However, the value simulated by Test 1 is approximately 60 W m^{-2} higher than the observed value. The result simulated by Test 2 is closer to the observed value but still approximately 30 W m^{-2} higher than the observed value. Test 3 is the best, and the simulated value is the closest to the observed value. The statistical results of each station are shown in Table 3. Test 3 has the lowest mean bias error (MBE) and the root mean square error (RMSE) between the simulated and observed shortwave flux results. The MBE of Test 3 is approximately 2–5 W m^{-2}, and the RMSE is approximately 10 W m^{-2}. Test 3 has the highest hit rate (HR, which is used to describe the accuracy of the model simulation; all above 0.72). Regarding the correlation coefficient (R), all tests show good consistency in the trend simulation (R=0.99). Therefore, Test 3 exhibits the best performance.

In addition, the model can better simulate the distribution characteristics of the wind, temperature and humidity. Figure 7 is a comparison of the horizontal distribution between the observed and simulated 2 m temperature, 2 m humidity and 10m wind speed. The analysis shows that in the daytime, the model has good simulation results for the temperature distribution. The simulated value of most stations is close to the observed value. However, at night, the simulated results of some suburban stations are higher and central stations are lower than the observed values. For the distribution of specific humidity, the model generates better simulation results during the day. However, at night, the simulation results in the central part of the city are lower, approximately 0.2–0.5 g kg^{-1}. For the wind results, the simulated and observed wind directions are consistent during the daytime, but the simulated wind speeds are higher than the observed values. At night, there are similar problems.

4. Aerosol effects on radiation and boundary layer

The atmospheric energy budget may change due to the change in the atmospheric extinction coefficient via aerosols. The reform of the energy budget will lead to changes in the PBL meteorological fields and further pollution development. In this section, we will focus on the influence of aerosols on the PBL meteorological fields, such as radiation, energy, temperature and boundary layer height. Furthermore, the influence of aerosols on radiation and boundary layers will be analyzed here.

4.1 Aerosol effects on shortwave radiation flux

Aerosols change the distribution of surface shortwave fluxes through scattering and absorption. Figure 8a and 8b show the horizontal distribution of surface shortwave fluxes at 1200 LST in the six-ring area of Beijing. The surface shortwave flux in the southern region is significantly smaller than that

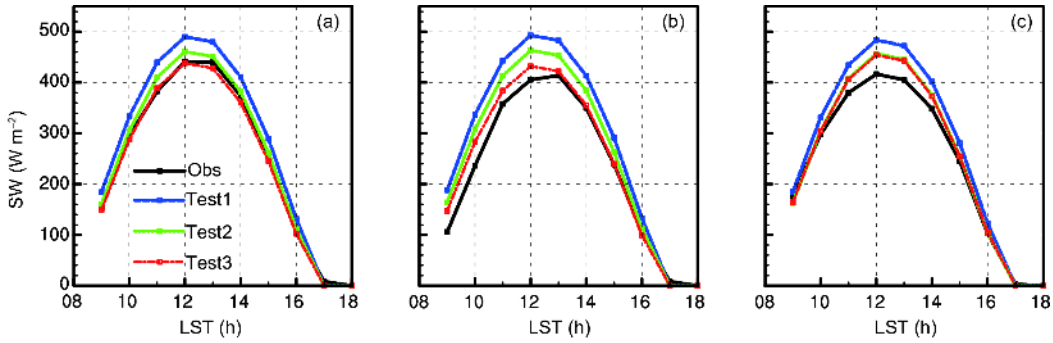

Figure 6 Diurnal variations in the surface short wave radiation flux at three sites ((a) IAP, (b) South Suburb Observatory, (c) Miyun) in Beijing. The black lines are the observation data, and the blue, green and red lines are the results from Test 1, Test 2, and Test 3, respectively.

Table 3 Statistics for the simulated and observed surface shortwave radiation flux from three numerical experiments

Sites	MBE (W m^{-2})			RMSE (W m^{-2})			*R*			HR (10 W m^{-2})		
	Test 1	Test 2	Test 3	Test 1	Test 2	Test 3	Test 1	Test 2	Test 3	Test 1	Test 2	Test 3
IAP	12.8	4	−2.3	23.4	8.7	6.4	0.99	0.99	0.99	0.6	0.8	0.8
South Suburb Observatory	23.1	14.1	5.6	43.1	27.9	14.7	0.99	0.99	0.99	0.6	0.8	0.8
Miyun	14.3	6.1	5.2	27.5	14.8	13.3	0.99	0.99	0.99	0.64	0.68	0.72

in the northern region when pollution occurred (Figure 8a), and the difference between the M zone and N zone is 15 W m^{-2}. However, the aerosol decreased the surface shortwave flux in the southern area by approximately 50% more than that in the north (Figure 8b) because the pollution is more severe in the southern area (Figure 4). The mean difference between the M zone and N zone is 24 W m^{-2}. The daily variations in the surface shortwave fluxes in the two zones are compared (Figure 8a), which indicates that there are obvious daily variations in the difference between them, and the variation is related to the change itself. The daily variation in $PM_{2.5}$ in the two zones indicates that the difference between the two areas is always between 100 and 350 μg m^{-3} except for the high values in the morning and low values at 1500 LST. These results combined with the analysis above indicate that aerosols have more important impacts on the surface shortwave flux and that the flux decrease is mainly related to the variation in shortwave radiation.

The vertical shortwave flux is affected by aerosols. Figure 9 shows a vertical section of the net shortwave flux. Figure 9a shows that aerosols gradually decreased the solar radiation fluxes reaching the ground. Therefore, the net shortwave flux also decreases with altitude. As the pollution decreases with altitude (Figure 5b), the change in the net shortwave flux between Test 3 and Test 1 also decreases with altitude, and the change at the ground reached 48 W m^{-2}. However, the vertical change in the net shortwave flux before and after pollution shows the opposite distribution (Figure 9b). The change is very small above 1 km, but it increases sharply from 1 km to the ground, especially below 500 m. The change reached 12–13W m^{-2} approximately 100 m from the ground. It is clear that the vertical distribution of the change in net shortwave radiation is consistent with the vertical aerosol extinction coefficient profile. Therefore, the presence of aerosols increases the absorption of the net shortwave flux near the surface and decreases it in the upper layer. The vertical change in the net shortwave flux changes the heating rate in the atmosphere. This result suggests that aerosols not only change the variation in the vertical net shortwave flux but also alter the atmospheric heating rate by changing the energy.

4.2 Effects of aerosol on the surface energy balance

Changes in incident shortwave fluxes result in varying sensible heat fluxes. The surface sensible heat flux is positive with values of 0–65 W m^{-2} in the six-ring area of Beijing when pollution occurs (Figure 10a), indicating that the surface temperature is higher than that in the atmosphere and that there is a large heat flux transferred from the surface to the atmosphere within the six-ring area. However, during the pollution event, the change in the sensible heat flux is negative (Figure 10b). Combined with Figure 4, where the AOD equals 0.4 at the boundary, the decline in the surface sensible heat flux in the southern region is 25–35 W m^{-2}, and in the northern region, this value is 15–25 W m^{-2}. The N zone declined by approximately 24 W m^{-2}, the M zone declined by approximately 15 W m^{-2}, and the mean difference between them is approximately 11 W m^{-2}. These results suggest that with high pollution, the ground temperature decreased, the sensible heat flux transmission declined, and the distribution of sensible heat flux changed significantly.

The surface latent heat flux changed significantly after pollution, and it is positive when pollution occurs; the value

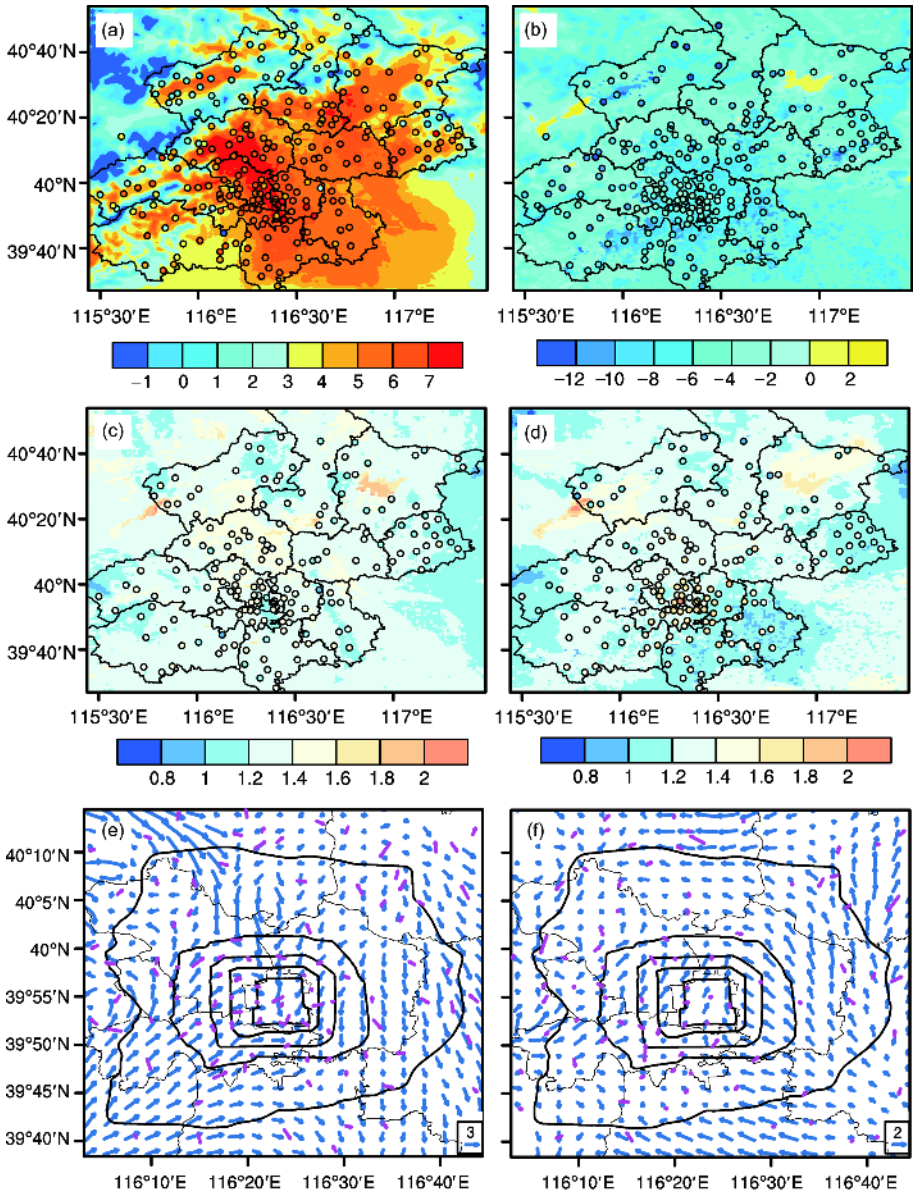

Figure 7 Comparison of horizontal distribution between the observed (dots) and simulated (shaded) temperature, humidity, and wind: (a) and (b) 2 m temperature (°C) at 1400 LST and 0200 LST respectively, (c) and (d) 2 m humidity (g kg^{-1}) at 1400 LST and 0200 LST respectively, (e) and (f) 10 m wind (m s^{-1}) at 1400 LST and 0200 LST respectively. The blue bars are the simulation results, and the pink bars are the observation results.

is small within the five-ring areas and gradually increases outside the five-ring area. However, with the influence of pollutants, the change in the surface latent heat flux declined by approximately 0–13 W m^{-2} in all six-ring areas. This result indicates that the surface latent heat flux is mainly related to the land use type and boundary layer turbulence structure, which has no obvious correlation with the distribution of aerosols.

4.3 Effects of aerosols on temperature

A change in energy will cause a change in temperature. Figure 11a shows the mean change in temperature during 1300–1500 LST. The temperature diminished by approximately 0–0.25°C due to aerosols in most of the six-ring areas. In the southern area, the temperature decreased by approximately 0.25–0.5°C (the temperature in the N zone decreased by approximately 0.29°C), but the change in temperature in the northern area was less than that in the southern area, except for the northwest area (the area is the location of Xiangshan Mountain, whose temperature is affected by the underlying surface and the terrain). The temperature in the M zone decreased by 0.16°C. Thus, the change in surface temperature between the north and south areas is different and is related to the AOD distribution. Figure 11b shows the average change in temperature at the

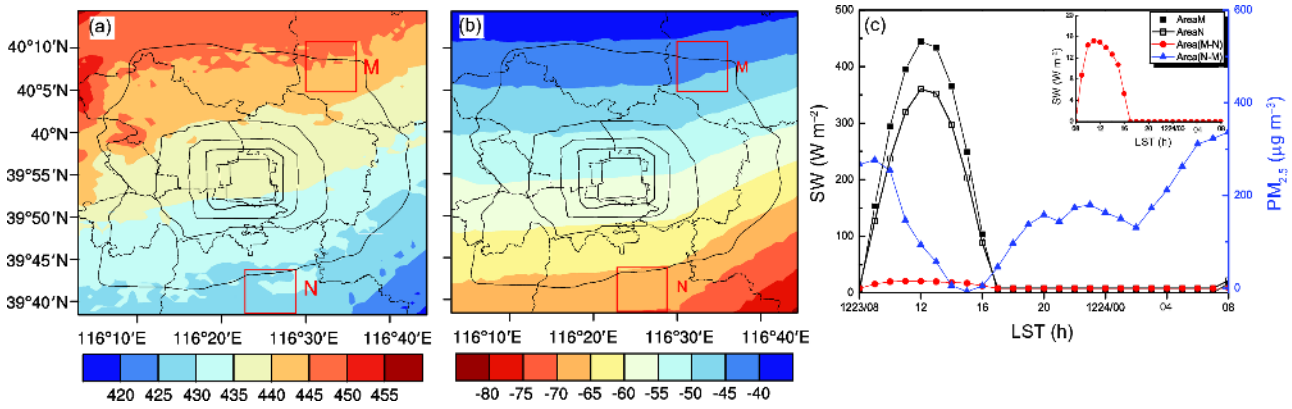

Figure 8 Temporal and horizontal distributions of surface shortwave radiation flux and daily variation in $PM_{2.5}$. (a) Surface shortwave radiation flux in Test 3, (b) the difference in surface shortwave radiation flux between Test 3 and Test 1, and (c) temporal change in surface shortwave radiation flux and its difference between zones M and N and the $PM_{2.5}$ difference between the two zones. The small figure is an enlarged version of the radiation difference.

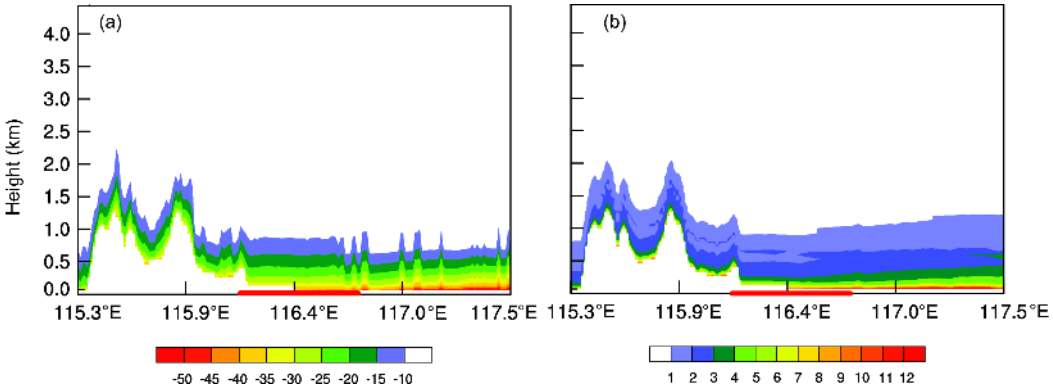

Figure 9 The vertical distribution of the net shortwave radiation flux (W m^{-2}) along the AB section (AB can be seen in Figure 1) at 1400 LST. (a) The difference in the net shortwave radiation between Test 3 and Test 1, (b) vertical gradient of (a).

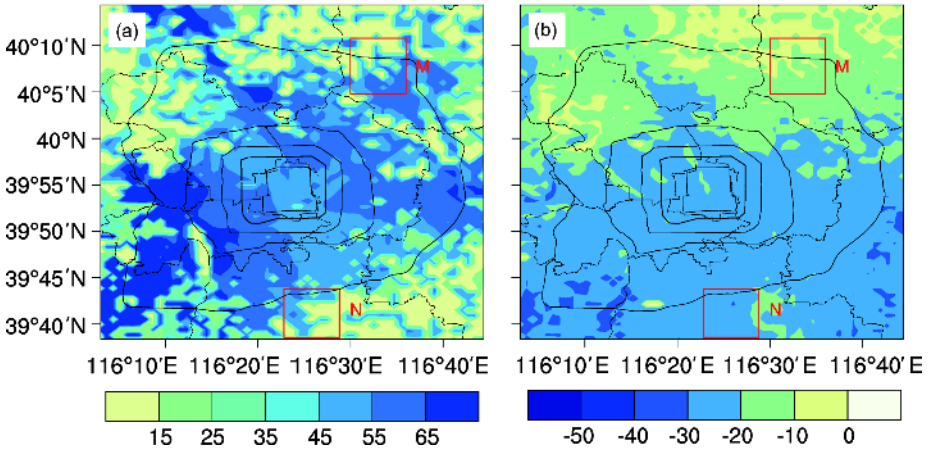

Figure 10 Horizontal distribution of mean sensible heat flux (g kg^{-1}) during 1300–1500 LST. (a) Test 3, (b) the difference between Test 3 and Test 1.

height of 950 hPa during 1300–1500 LST. The temperature is mainly increased throughout the six-ring area due to aerosols. The temperature increased by approximately 0–0.3°C in the northern area, increased by more than 0.6°C in most parts of the southern area, and in some areas, the change in temperature was greater than 0.9°C. This result indicates that the temperature in the southern area increases significantly more than that in the northern area at the 950 hPa level. The increase in average temperature in the N zone is 0.44°C, and in the M zone, this value is only 0.12°C; the difference between them is 0.32°C.

The vertical temperature change can better explain the

effect of aerosols on temperature. As shown in Figure 12a, the increase in temperature in the vertical direction reaches a maximum value within 1 km due to aerosols, and the closer to surface, the greater the temperature increase. However, the temperature begins to decrease due to atmospheric pollutants at approximately 200 m. In the WRF model, the change in vertical temperature is mainly determined by the change in the atmospheric heating rate. The results from part 4.1 indicate that the change in the atmospheric heating rate is directly related to the vertical change in the net shortwave flux, so the change in temperature is determined by the change in the net shortwave radiation, and this change is related to the distribution of aerosols. Therefore, the vertical distribution of AOD leads to a vertical change in the net shortwave flux, which increases the temperature in the upper PBL. However, as the incident shortwave flux decreased due to the large amounts of aerosol, the net shortwave flux near the ground decreased, and the temperature of the lower PBL also decreased. Therefore, the stability of the atmosphere was enhanced. This result suggests that aerosols, radiation and temperature have a strongly corresponding relation, which is consistent with the results of Wang et al. (2015a, 2015b); and Gao et al. (2015).

Figures 12b and 12c compare the temperature distributions of the two regions. The analysis shows that the temperature of the N zone with severe pollution declined (over 0.5°C) near the surface and greatly increased in the upper layer (over 0.4°C). The temperature in the M zone where the pollution was slight declined by only approximately 0.2°C near the surface and increased by approximately 0.2°C in the upper layer. Therefore, the temperature changes caused by aerosols in the southern area where the pollution is severe will increase the stability of atmospheric stratification, which further verifies the conclusions above.

4.4 Aerosol effects on boundary layer height

Changes in atmospheric stratification result in a varying planet boundary layer height (PBLH). Figure 13 shows the horizontal distribution of the PBLH during 1300–1500 LST. We find that the PBLH within the six-ring area is below 900m when pollution occurs (Figure 13a). There is a high boundary layer of 800–900 m at the city center, which is mainly due to the existence of a high wind speed zone in this area. The change in the PBLH (Figure 13b) indicates that the height of the boundary layer decreases within the six-ring

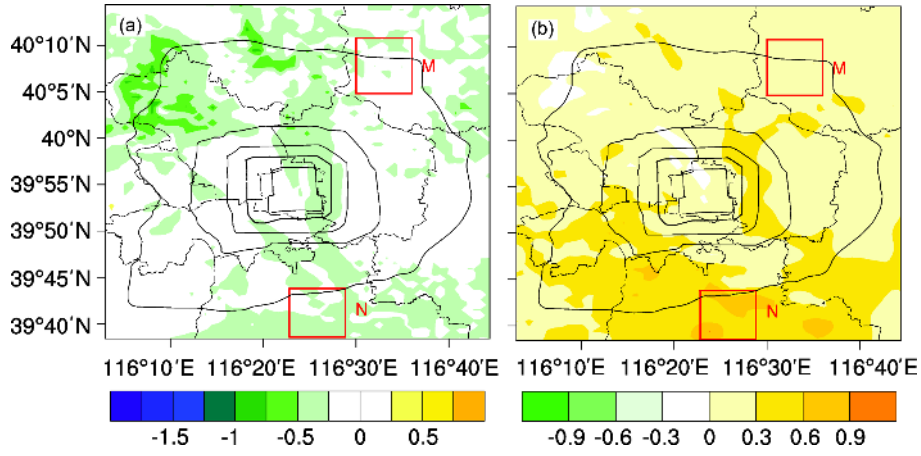

Figure 11 Horizontal distribution of mean temperature (°C) during 1300–1500 LST. (a) Test 3, (b) the difference between Test 3 and Test 1.

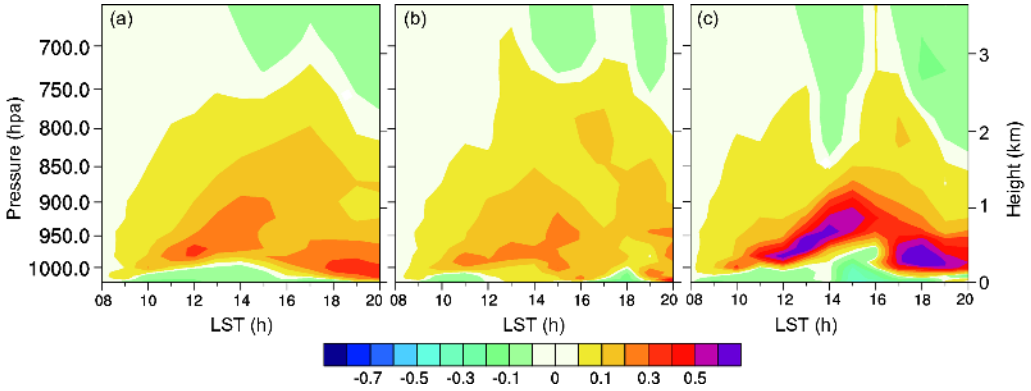

Figure 12 Daily variations in mean temperature differences (°C) between Test 3 and Test 1. (a) Six-ring area in Beijing, (b) M zone, and (c) N zone.

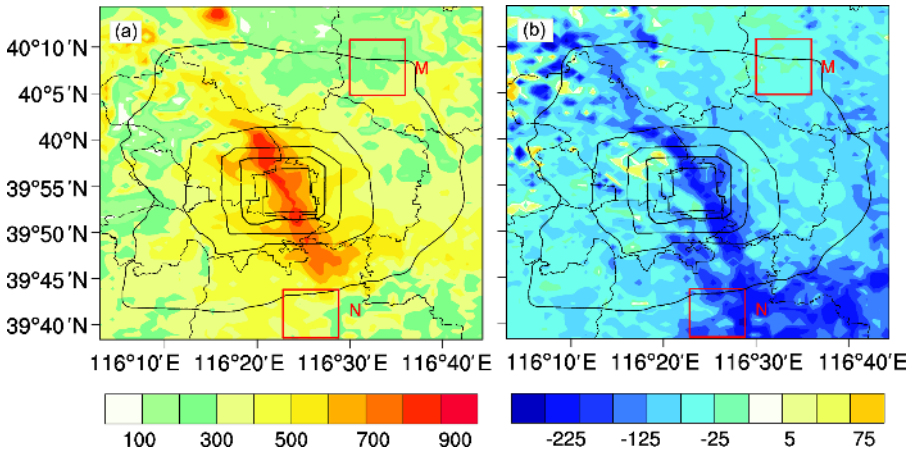

Figure 13 Horizontal distribution of the mean PBLH (m) during 1300–1500 LST. (a) Test 3, (b) Differences between Test 3 and Test 1.

region during the day, and the maximum reduction reached approximately 425 m. The reduction is mainly related to the distribution characteristics. Therefore, aerosols decreased the PBLH, and the southern area exhibited the largest reduction. The M zone was compared with the N zone, which revealed that the PBLH decreased by approximately 184 m in the southern area and only 42 m in the northern area. The difference between these two areas is greater than 14 m. The result show that the PBLH was significantly reduced by AOD and the reduction was mainly related to its own distribution characteristics.

5. Numerical experiments of aerosol radiative forcing on urban boundary layer

In this part, we select three key parameters of the urban boundary layer and conduct numerical experiments introduced in part 2.2 to discuss the effects of aerosol radiative forcing, underlying urban surfaces and the combination of both on the characteristics of the urban boundary layer.

5.1 The variation in urban heat island intensity

Urban heat island intensity (UHII) is the difference between the average temperature within the five-ring sites below 300 m and the average temperature outside of the five-ring sites below 300 m. The daily variation in the UHII in the different numerical experiments is shown in Figure 14. The UHII varies from −3.8 to 2°C during 0800–2000 LST. And it increases slightly and then decreases after sunrise. After 1100 LST, the UHII again increases until 1600 LST when it reaches a maximum and then further decreases. The UHII values from different experiments were compared, which indicated that the UHII increases gradually due to the absorption of solar radiation by aerosols before 1100 LST. The larger AOD is, the more solar radiation is absorbed, and the stronger UHII is. Taking 0900 LST as an example, when the MODIS-AOD increases from 0 to two and four times, the UHII values increase by 0.2 and 0.4°C, respectively. After 1100 LST, the larger the AOD is, the more solar radiation is scattered, and the weaker UHII is. At 1500 LST, the UHII of Test 9 is 0.8°C and of Test 7 and Test 4 is 1.2 and 1.3°C, respectively. The change in UHII decreases with increasing AOD. After sunset (1700–2000 LST), the underlying surface of the city cools slowly, and the suburb area cools quickly. Together with the high AOD in the city, the surface cools more slowly, and its UHII is stronger.

5.2 The variation in atmospheric stability

To discuss the change in atmospheric stratification stability quantitatively, three sites are selected here. These sites are the IAP station, South Suburb Observatory station and Tongzhou station, which are high-density urban stations, low-density urban stations (also known as suburban stations) and rural stations, respectively. The locations are shown in Figure 3. Figure 15 shows the vertical profiles of the potential temperatures of the three sites under different AODs. With the increase in AOD, the surface temperature of the IAP station decreases gradually, and the high-level temperature increases (Figure 15a). When the AOD increases to 4.5 times MODIS-AOD (Test 8 and AOD=1.5), the atmospheric stratification changes from unstable to neutral. As the AOD continues to increase, the neutral atmosphere remains almost unchanged. Figure 15b shows the vertical profile of the South Suburb Observatory Station. As the AOD increased, the surface temperature decreased significantly. When AOD increased to 3.5 times MODIS-AOD (Test 6 and AOD=1.39), the atmospheric stratification began to change from unstable to stable, and with the increase in AOD, it became stronger. Figure 15c shows the vertical profile of the Tongzhou station, which is similar to that of Figure 15a and 15b. When AOD increases to 3.5 times MODIS-AOD (this is

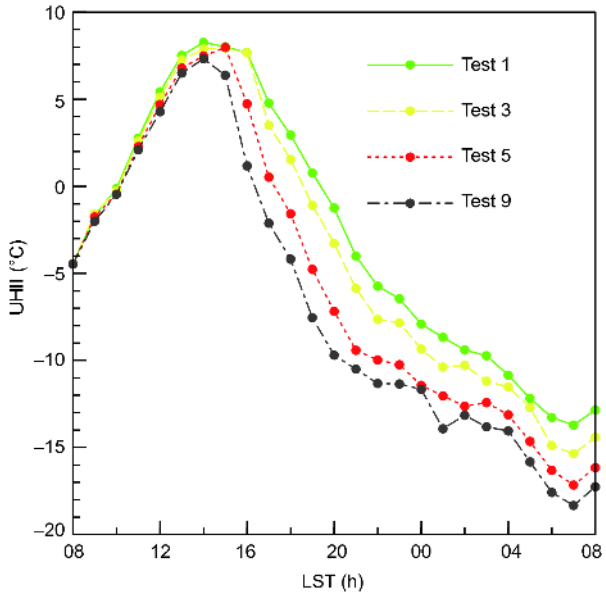

Figure 14 Daily variations in simulated UHII (°C) in different numerical experiments.

Test6 and AOD=1.35), the atmospheric stratification becomes stable, and with the increase in AOD, it is enhanced significantly.

These results suggest that due to the underlying surface of the city, the atmospheric stratification of the IAP station, which is in a high-density urban area, changes from unstable to neutral when the AOD increases to 1.5, but stable stratification is not easily formed. When the AOD increases to 1.39, the atmospheric stratification at the South Suburb Observatory station, which is in the low-density urban area, begins to change, and it more easily becomes stable. For the rural Tongzhou station, the stratification will change from unstable to stable only when the AOD increased to 1.35, and with the increase in the AOD, the stability significantly enhances, which means that the atmospheric stratification is most likely to become stable in this area.

Figure 16 clearly indicates that the atmospheric stratification at the three sites is unstable without pollution. When aerosols increase to 3.5 times the initial value (Test 6), the atmospheric stratification at the rural site first changes from unstable to moderate stability, while the atmospheric stratification at the suburban site changes from unstable to weakly stable, and the urban site remains unstable. When aerosols continue to increase to 4.5 times the initial value (Test 8), the atmospheric stratification at the rural site changes from moderate stability to strong stability, the suburban site begins to change from weak stability to strong stability, and the urban site changes from unstable to neutral. Finally, when aerosols increase to 5 times the initial value (Test 9), the atmospheric stratification of the urban site remains neutral, and the stability is difficult to change. The atmospheric stratification of the suburban station and the rural station remain stable, but that at the rural station is stronger. Therefore, the difference in the roughness of the underlying surface will have different impacts on the stability of the atmosphere, and there is a certain correlation between urbanization and atmospheric stratification under different aerosol concentrations.

5.3 The variation in the 2 m temperature

Figure 17 shows the change in the 2 m temperature under different numerical experiments. Three sites are selected for comparison. They are the IAP station, the South Suburb Observatory station and the Tongzhou station. Among these stations, the AOD of the South Suburb Observatory station is the highest, followed by that of the Tongzhou station, and the AOD of the IAP station is the lowest. Figure 17 indicates that with the increase in the AOD, the change in the 2 m temperature at the three sites increases gradually. Because the IAP station has the highest surface albedo, its temperature and temperature variations are the largest before the AOD increases to 3.5 times the initial value (Test 6). However, when the AOD exceeds the initial value by 3.5 times (Test 6), the temperature of the South Suburb Observatory station, which has low albedo, is greater than that at the IAP station due to the increase in AOD. The Tongzhou station has a stable temperature due to the limited number of pollutants and the lowest albedo of the underlying surface. This result

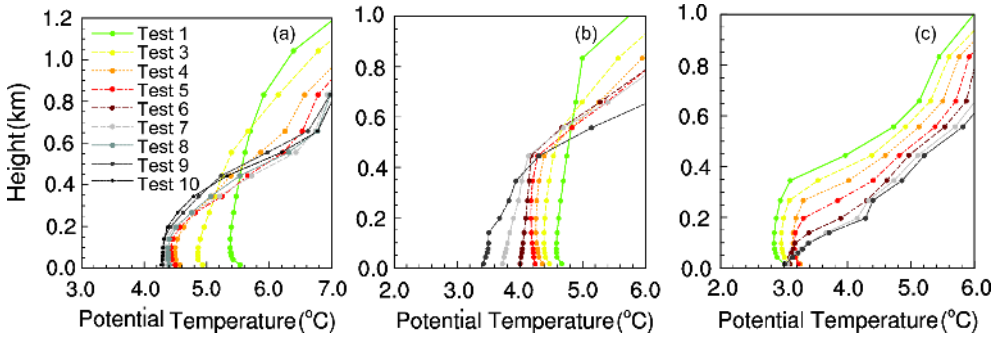

Figure 15 Vertical profiles of potential temperature in different numerical experiments at 1400 LST. (a) IAP station, (b) South Suburb Observatory station, (c) Tongzhou station.

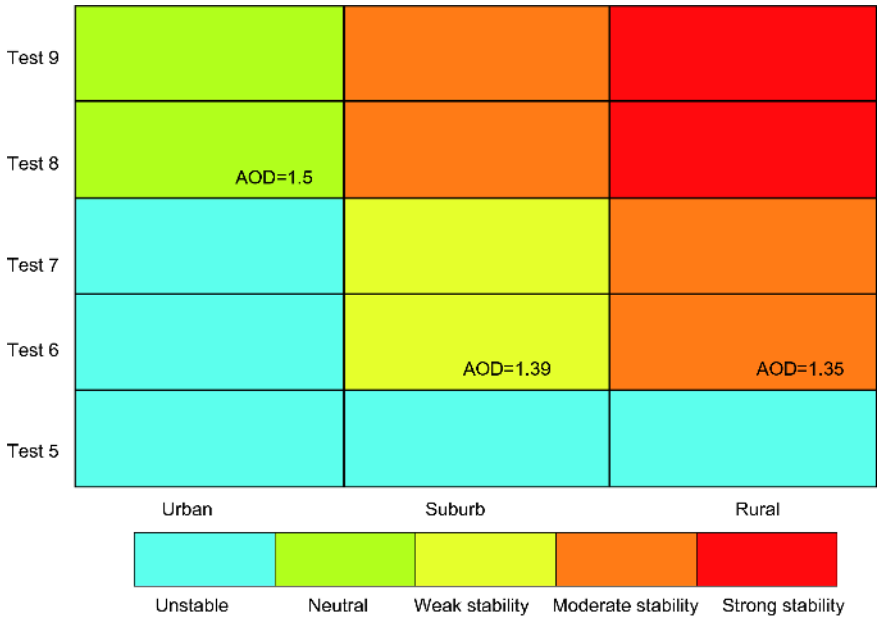

Figure 16 Relationship between atmospheric stratification and urbanization under different AODs.

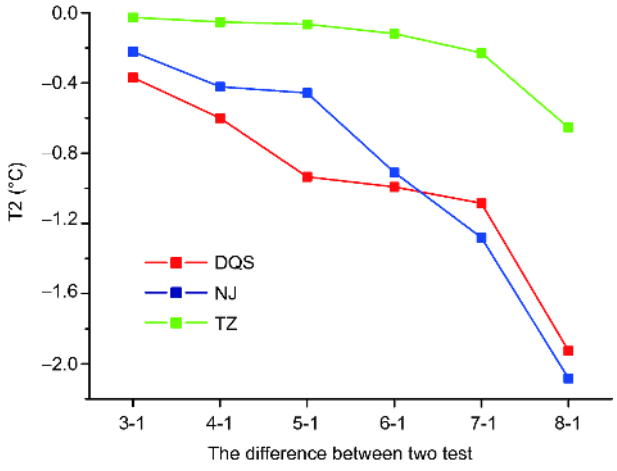

Figure 17 Variations in 2 m temperature (°C) at 1400 LST in different numerical experiments.

shows that the change in the 2 m temperature is different from the change in the UHII and atmospheric stratification stability. This change is affected by two factors: AOD and underlying urban surface. Therefore, it is necessary to analyze the changes in PBL meteorology by combining pollution and underlying urban surfaces in future research.

6. Conclusion and discussion

With the intensification of pollution and urbanization, the aerosol radiation effect continues to play an important role in the urban boundary layer. The winter pollution process in Beijing is taken as an example, and the optimization of the WRF model-V3.7 is targeted. This paper introduces a vertical aerosol profile and optimizes the radiation parameterization scheme. Based on the validity of the optimization scheme, the characteristics of the PBL meteorology during the pollution period are simulated, and the influence of aerosols on radiation and the PBL is analyzed. Finally, the effects of aerosols and the underlying surfaces on atmospheric stratification and diffusion conditions are discussed by using a series of numerical experiments. The results show the following:

(1) The optimized WRF model can better simulate the incident shortwave radiation flux and the horizontal distribution of temperature, humidity and wind in Beijing.

(2) By analyzing the relationship between aerosols and PBL meteorology, the study finds that aerosols warm the upper PBL by increasing the change in the vertical variation in net shortwave radiation flux (heating rate of the atmosphere) and cools the surface temperature by reducing the surface shortwave radiation flux. Therefore, the atmospheric stratification becomes more stable, and the height of the boundary layer is lower, which reduces the energy transmission and the wind speed.

(3) The aerosol radiation effect, the underlying urban surfaces and the combination of the two are the main reasons for the change in PBL meteorology. Under the influence of the aerosol radiation effect, the UHII decreases during the day, and the rate decreases with increasing AOD. Under the influence of the underlying urban surfaces, when the AOD increases to 3.5 times the initial value, the urban atmospheric stratification remains unstable, and the atmospheric stratification in rural areas (AOD=1.35) and suburbs (AOD=1.39) begins to become stable, and this stability is stronger in the rural areas. When the AOD value increases to 4.5 times the

initial value, the atmospheric stratification in rural areas is strongly stable, the suburb area is moderately stable, and the urban area is neutral. When the AOD increases to 9 times the initial value, the three regions maintain the current conditions with no change. Under the effects of both aerosol radiation and underlying urban surfaces, the 2 m temperature shows different characteristics when the AOD increased to 3 times the initial value. Therefore, it is necessary to comprehensively analyze the changes in the urban boundary layer by combining the characteristics of pollution and the underlying urban surfaces in subsequent research.

Most of the discussions are based on AOD, and the daily variation in AOD is not considered in this paper; therefore, it is necessary to consider aerosol optical characteristics when analyzing the influence of the AOD and further improving the WRF model to discuss the relationships among aerosols, radiation, the boundary layer and the underlying surfaces.

Acknowledgements *Thanks to Quan Jiannong, Sun Zhaobin, Gao Hua, Zhang Yizhou, Dou Jingjing from Beijing Meteorological Institute of China Meteorological Administration, and Michael Barlage from the National Center for Atmospheric Research for their assistance in data collection and processing. This work was supported by the Ministry of Science and Technology of China (Grant No. 2015DFA20870) and the Beijing Municipal Science and Technology Commission (Grant Nos. D171100000717003, Z161100001116065 & Z151100002115045).*

References

Albrecht B A. 1989. Aerosols, cloud microphysics, and fractional cloudiness. Science, 245: 1227–1230

Beljaars A C M. 1995. The parametrization of surface fluxes in large-scale models under free convection. Q J R Met Soc, 121: 255–270

Che H Z, Xia X G, Zhu J, Wang H, Wang Y Q, Sun J Y, Zhang X Y, Shi G Y. 2015. Aerosol optical properties under the condition of heavy haze over an urban site of Beijing, China. Environ Sci Pollut Res, 22: 1043–1053

Che H, Shi G, Uchiyama A, Yamazaki A, Chen H, Goloub P, Zhang X. 2008. Intercomparison between aerosol optical properties by a PREDE skyradiometer and CIMEL sunphotometer over Beijing, China. Atmos Chem Phys, 8: 3199–3214

Chen F, Kusaka H, Bornstein R, Ching J, Grimmond C S B, Grossman-Clarke S, Loridan T, Manning K W, Martilli A, Miao S, Sailor D, Salamanca F P, Taha H, Tewari M, Wang X, Wyszogrodzki A A, Zhang C. 2011. The integrated WRF/urban modelling system: Development, evaluation, and applications to urban environmental problems. Int J Climatol, 31: 273–288

Cheng Y, Canuto V M, Howard A M. 2002. An improved model for the turbulent PBL. J Atmos Sci, 59: 1550–1565

Ding A J, Fu C B, Yang X Q, Sun J N, Petäjä T, Kerminen V M, Wang T, Xie Y, Herrmann E, Zheng L F, Nie W, Liu Q, Wei X L, Kulmala M. 2013. Intense atmospheric pollution modifies weather: A case of mixed biomass burning with fossil fuel combustion pollution in eastern China. Atmos Chem Phys, 13: 10545–10554

Dong F, Wang X Q, Wang Z F, Yan P Z. 2013. A study of the north-south differences of the air quality in Beijing (in Chinese). Climat Environ Res, 59: 3996–4006

Dou J J. 2013. Fine-Scale Characteristics of Low-Level Meteorological Elements in Beijing Urban Area (in Chinese). Beijing: Chinese Academy of Meteorological Sciences

Dyer A J, Hicks B B. 1970. Flux-gradient relationships in the constant flux layer. Q J R Met Soc, 96: 715–721

Gao Y P, Zhang M G, Liu Z R, Wang L C, Wang P, Xia X A, Tao M H, Zhu L. 2015. Modeling the feedback between aerosol and meteorological variables in the atmospheric boundary layer during a severe fog-haze event over the North China Plain. Atmos Chem Phys, 15: 4279–4295

Huang J P, Minnis P, Lin B, Wang T H, Yi Y H, Hu Y X, Sun-Mack S, Ayers K. 2006. Possible influences of Asian dust aerosols on cloud properties and radiative forcing observed from MODIS and CERES. Geophys Res Lett, 33: L06824

Huang X, Ding A J, Liu L X, Liu Q, Ding K, Niu X R, Nie W, Xu Z, Chi X G, Wang M H, Sun J N, Guo W D. 2016. Effects of aerosol-radiation interaction on precipitation during biomass-burning season in East China. Atmos Chem Phys, 16: 10063–10082

Iacono M J, Delamere J S, Mlawer E J, Shephard M W, Clough S A, Collins W D. 2008. Radiative forcing by long-lived greenhouse gases: Calculations with the AER radiative transfer models. J Geophys Res, 113: D13

Kain J S. 2004. The Kain-Fritsch convective parameterization: An update. J Appl Meteorol, 43: 170–181

Li J X, Qiu Q H, Xin L Z, Sun F, Li L J. 2007. The characteristics and cause analysis of heavy air pollution in autumn and winter in Beijing (in Chinese). Environ Monitor China, 23: 92–97

Li L Q, Zhou M Y, Li X S. 1992. The interaction between nocturnal urban atmospheric boundary layer and aerosols (in Chinese). J Appl Meteor Sci, 3: 32–41

Li Y K, Chao J P, Kuang G X. 2015. Dynamic and thermodynamic analysis of the urban heat island effect and aerosol concentration (in Chinese). Chin J Geophys, 58: 729–740

Li Z Q, Guo J P, Ding A J, Liao H, Liu J J, Sun Y, Wang T J, Xue H W, Zhang H S, Zhu B. 2017. Aerosol and boundary-layer interactions and impact on air quality. Natl Sci Rev, 4: 810–833

Liao J B. 2014. Study on meteorological factors and air quality due to urbanization in the Yangtze River Delta (YRD), China (in Chinese). Doctor Dissertation. Nanjing: Nanjing University

Liu P F, Zhao C S, Zhang Q, Deng Z Z, Huang M Y, Ma X C, Tie X X. 2009. Aircraft study of aerosol vertical distributions over Beijing and their optical properties. Tellus B-Chem Phys Meteor, 61: 756–767

Liu Y, Liu H Z, Wang L. 2017. The vertical distribution characteristics of integral turbulence statistics in the atmospheric boundary layer over an urban area in Beijing. Sci China Earth Sci, 60: 1533–1545

Pandithurai G, Seethala C, Murthy B S, Devara P C S. 2008. Investigation of atmospheric boundary layer characteristics for different aerosol absorptions: Case studies using CAPS model. Atmos Environ, 42: 4755–4768

Paulson C A. 1970. The mathematical representation of wind speed and temperature profiles in the unstable atmospheric surface layer. J Appl Meteorol, 9: 857–861

Pleim J E. 2007. A Combined local and nonlocal closure model for the atmospheric boundary layer. Part I: Model description and testing. J Appl Meteorol Climatol, 46: 1383–1395

Su T, Miao J F, Cai Q B. 2016. A numerical simulation of sea breeze thunderstorm structure over the Hainan island (in Chinese). Chin J Geophys, 59: 59–78

Sun D, Duan M, Lv D, Wang P, Wang H, Zhang X. 2012. Impact of different aerosols on the evolution of the atmospheric boundary layer. Atmos Ocean Sci Lett, 5: 82–87

Tang H, Jia L H. 2006. Brief introduction of American ARW model system (in Chinese). Xinjiang Meteorol, 29: 24–26

Tao W, Liu J F, Tao S. 2014. Effects of urban underlying surface change on ambient atmospheric environment (in Chinese). Tropical Geog, 34: 283–292

Tewari M, Chen F, Wang W, Dudhia J, LeMone M A, Mitchell K, Ek M, Gayno G, Wegie J, Cuenca R H. 2004. Implementation and verification of the unified NOAH land surface model in the WRF model. In: 20th Conference on Weather Analysis and Forecasting/16th Conference on Numerical Weather Prediction. 1115

Thompson G, Field P R, Rasmussen R M, Hall W D. 2008. Explicit

forecasts of winter precipitation using an improved bulk microphysics scheme. Part II: Implementation of a new snow parameterization. Mon Weather Rev, 136: 5095–5115
Wang H, Shi G Y, Zhang X Y, Gong S L, Tan S C, Chen B, Che B, Li T. 2015a. Mesoscale modelling study of the interactions between aerosols and PBL meteorology during a haze episode in China Jing-Jin-Ji and its near surrounding region—Part 2: Aerosols' radiative feedback effects. Atmos Chem Phys, 15: 3277–3287
Wang H, Xue M, Zhang X Y, Gong S L, Tan S C, Chen B, Che B, Li T. 2015b. Mesoscale modeling study of the interactions between aerosols and PBL meteorology during a haze episode in Jing-Jin-Ji (China) and its nearby surrounding region—Part 1: Aerosol distributions and meteorological features. Atmos Chem Phys, 15: 3257–3275
Wang J T, Zhang L, Zhang B K, Cao X J, Wang H B. 2013. The impacts of urban underlying surface on the winter urban heat island effect and the boundary layer structure over the valley city Lanzhou (in Chinese). J Meteorol Res, 71: 1115–1129
Wang J, Christopher S A, Nair U S, Reid J S, Prins E M, Szykman J, Hand J L. 2006. Mesoscale modeling of Central American smoke transport to the United States: 1. "Top-down" assessment of emission strength and diurnal variation impacts. J Geophys Res, 111: D05S17
Wang X Q. 2017. Numerical simulation study on the influence of urban underlying surface on precipitation process in Beijing-Tianjin-Hebei (in Chinese). Nanjing: Nanjing University of information Science & Technology
Wang X R, Miao S G, Dou J X, Dong F, Wang J L. 2016. Observation and analysis of the air pollution impacts on radiation balance of urban and suburb areas in Beijing (in Chinese). Chin J Geophys, 59: 3996–4006
Webb E K. 1970. Profile relationships: The log-linear range, and extension to strong stability. Q J R Met Soc, 96: 67–90
Wong D C, Pleim J, Mathur R, Binkowski F, Otte T, Gilliam R, Pouliot G, Xiu A, Young J O, Kang D. 2012. WRF-CMAQ two-way coupled system with aerosol feedback: Software development and preliminary results. Geosci Model Dev, 5: 299–312
Wu D, Liao B T, Wu M, Chen H Z, Wang Y C. 2014. The long-term trend of haze and fog days and the surface layer transport conditions under haze weather in North China (in Chinese). Environ Sci-China, 34: 1–11
Yu H, Liu S C, Dickinson R E. 2002. Radiative effects of aerosols on the evolution of the atmospheric boundary layer. J Geophys Res, 107: 4142
Zhang D, Anthes R A. 1982. A high-resolution model of the planetary boundary layer—Sensitivity tests and comparisons with SESAME-79 data. J Appl Meteorol, 21: 1594–1609
Zhang Q, Ma X C, Tie X X, Huang M Y, Zhao C S. 2009. Vertical distributions of aerosols under different weather conditions: Analysis of *in-situ* aircraft measurements in Beijing, China. Atmos Environ, 43: 5526–5535
Zhang Y Z, Miao S G, Dai Y J, Liu Y H. 2013. Numerical simulation of characteristics of summer clear day boundary layer in Beijing and the impact of urban underlying surface on sea breeze (in Chinese). Chin J Geophys, 56: 2558–2573
Zhao L, Lv S H, Chen Y C, Ao Y H, Ma D, Bao Y. 2014. Simulation of summer radiation feature over badain jaran desert (in Chinese). Acta Energ Solar Sin, 35: 338–344

(Responsible editor: Chao LIU)